



# Variable Crustal Production Originating From Mantle Source Heterogeneity Beneath the South East Indian Ridge and Amsterdam-St. Paul Plateau

A.L.R. Sibrant, M. Maia, E. Mittelstaedt, D.W. Graham

## ► To cite this version:

A.L.R. Sibrant, M. Maia, E. Mittelstaedt, D.W. Graham. Variable Crustal Production Originating From Mantle Source Heterogeneity Beneath the South East Indian Ridge and Amsterdam-St. Paul Plateau. *Geochemistry, Geophysics, Geosystems*, 2019, 20, pp.4635 - 4653. 10.1029/2019GC008419 . hal-02379205

**HAL Id: hal-02379205**

**<https://hal.univ-brest.fr/hal-02379205>**

Submitted on 13 Apr 2021

**HAL** is a multi-disciplinary open access archive for the deposit and dissemination of scientific research documents, whether they are published or not. The documents may come from teaching and research institutions in France or abroad, or from public or private research centers.

L'archive ouverte pluridisciplinaire **HAL**, est destinée au dépôt et à la diffusion de documents scientifiques de niveau recherche, publiés ou non, émanant des établissements d'enseignement et de recherche français ou étrangers, des laboratoires publics ou privés.

# Geochemistry, Geophysics, Geosystems

## RESEARCH ARTICLE

10.1029/2019GC008419

### Key Points:

- Crustal architecture of the Amsterdam-St. Paul Plateau records high- and low-plume flux stages during mantle plume-spreading ridge interaction
- Plume magma flux decreased earlier in the south than in the north along a single spreading segment
- Along-axis differences in crustal thickness and Pb and He isotopes suggest both shallow mantle and plume heterogeneities

### Supporting Information:

- Supporting Information S1

### Correspondence to:

A. L. R. Sibrant,  
aurore.sibrant@u-psud.fr

### Citation:

Sibrant, A. L. R., Maia, M., Mittelstaedt, E., & Graham, D. W. (2019). Variable crustal production originating from mantle source heterogeneity beneath the South East Indian Ridge and Amsterdam-St. Paul Plateau. *Geochemistry, Geophysics, Geosystems*, 20, 4635–4653. <https://doi.org/10.1029/2019GC008419>

Received 29 APR 2019

Accepted 9 SEP 2019

Accepted article online 15 OCT 2019

Published online 5 NOV 2019

## Variable Crustal Production Originating From Mantle Source Heterogeneity Beneath the South East Indian Ridge and Amsterdam-St. Paul Plateau

A.L.R. Sibrant<sup>1</sup> , M. Maia<sup>2</sup>, E. Mittelstaedt<sup>3</sup> , and D.W. Graham<sup>4</sup>

<sup>1</sup>Laboratoire Géosciences Océan, University of Brest, Plouzané, France, <sup>2</sup>Laboratoire Géosciences Océan, CNRS, University of Brest, Plouzané, France, <sup>3</sup>Department of Geological Sciences, University of Idaho, Moscow, ID, USA, <sup>4</sup>College of Earth, Ocean, and Atmospheric Sciences, Oregon State University, Corvallis, OR, USA

**Abstract** The Amsterdam-St. Paul (ASP) Plateau formed by interaction between the South East Indian Ridge (SEIR) and the ASP mantle plume during the last 10 Myr. The combined bathymetry and gravity-derived crustal thickness anomalies along the present and paleoaxes of the SEIR atop the plateau indicate: (1) a thicker crust and shallower water depth along the southern part of segment I2 during much of the last 10 Myr; (2) an earlier decrease (~1.4 Ma) in crustal thickness along the southern part of I2 compared to the northern part (~0.9 Ma) during the most recent period of reduced magmatism; (3) a topographic transition at ~0.7 Ma and during the last 0.1 Myr; and (4) an approximately uniform crustal thickness (8 km) along the entire I2 segment today. These observations require spatial and temporal variations in magma production during construction of the ASP Plateau over the last 3 Myr. We propose that during periods of weaker plume magma flux, spatial variations in upper mantle temperature and composition are small, and lead to small variations in crustal thickness along-axis. In contrast, during periods of stronger plume magma flux, spatial contrasts in upper mantle temperature and composition (fertility) are large, leading to significant variations in crustal thickness. Along-axis variations of <sup>3</sup>He/<sup>4</sup>He, Δ8/4Pb, K/Ti, and Na<sub>8</sub> in “zero-age” basalts indicate that there is a gradient in the underlying mantle material, from a “common” mantle plume component (Δ8/4Pb~60) stronger in the north to a DUPAL component (Δ8/4Pb~110) dominating in the south.

## 1. Introduction

Mantle hot spots have long been known to interact with nearby spreading centers and the overlying lithosphere (e.g., Ito et al., 2003; Morgan, 1978). When enough mantle hot spot material is drained toward the ridge axis, a large increase in crustal production can lead to the construction of oceanic plateaus such as Iceland (e.g., Johnson et al., 1972) and the Azores (e.g., Gente et al., 2003). Much of our understanding of mantle plume-spreading ridge interactions comes from the morphologic evolution of oceanic plateaus over time scales of a few millions to tens of millions of years (Schilling, 1985, 1991).

Indeed, the physical (size, morphology, structure) and geochemical characteristics of ridge-related oceanic plateaus depend on the strength of the interaction between plume and ridge and, thus, on the characteristics of both (e.g., Ito et al., 2003; Morgan, 1978; Vogt, 1976). For example, variations in plume magma supply (Allen et al., 2002; Cannat et al., 1999; Maia et al., 2000, 2007) can modify subaxial mantle temperature (Klein & Langmuir, 1987; McKenzie, 1984), axial morphology (Canales et al., 1997; Phipps Morgan & Chen, 1993), and segment length (e.g., Hey et al., 1977; Karsten & Delaney, 1989), as well as potentially promote ridge jumps toward nearby plumes (Hardarson et al., 1997; Maia et al., 2011; Mittelstaedt et al., 2011). Moreover, oceanic plateau basalts are commonly more enriched in incompatible elements (such as K or Na) and show distinct Sr, Pb, and He isotopic signatures compared to mid-ocean ridge basalts (Schilling, 1985; Schilling et al., 1982). Thus, the study of ridge-related oceanic plateaus also provides a means to evaluate the origin of these magmatic features and gain insight into the dynamics of plume-ridge interaction and mantle heterogeneity. However, information on finer time-scale resolutions (submillion year scales) of ridge-plume interactions and plateau evolution is far less frequent.

The 10-Myr-old Amsterdam-St. Paul (ASP) Plateau (Figure 1) lies along the intermediate spreading (full rate of 65 mm/year) South East Indian Ridge (SEIR). It is located astride two short ridge segments (I1 and J1, 20,

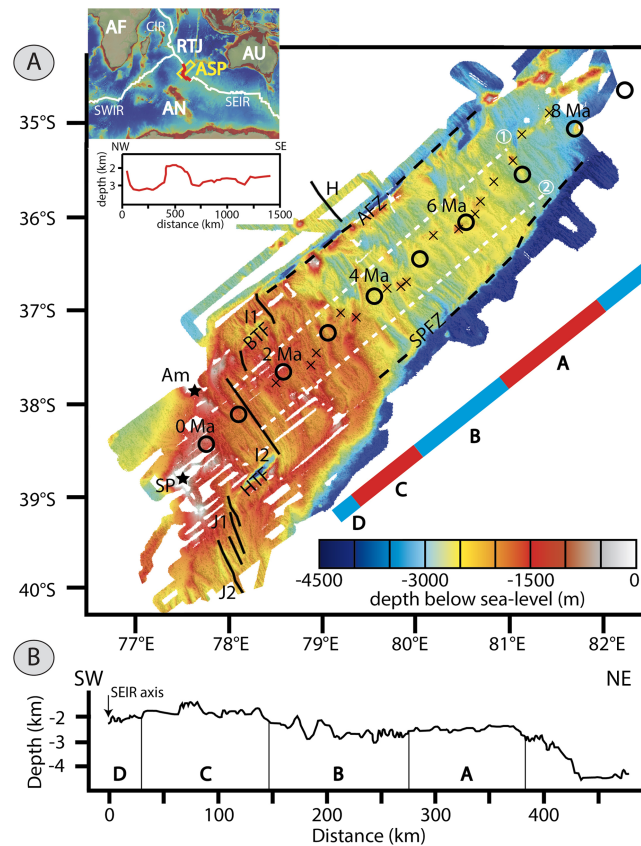


**Figure 1.** (a) Bathymetric map of the Amsterdam-St. Paul Plateau based on multibeam data from Maia et al. (2011) and the regional map with depth anomaly (inset). The ASP plume has been approaching (black circles show approximate locations since 9 Ma) the SEIR (thin, black lines) for >10 Ma. Interaction between the two resulted in alternating periods of greater (red blocks) and lesser (blue blocks) axial crustal production. The ASP plateau formed primarily along the segment I2 of the ridge axis between the Amsterdam Fracture Zone (AFZ) and the St. Paul Fracture Zone (SPFZ; dashed lines), while the Boomerang Transform Fault (BTf) recently formed within the zone of enhanced volcanism. The Hillegom Transform Fault (HTf) is the remaining active portion of the SPFZ. Small volcanoes (crosses) have formed consistently near the center of Segment I2 until ~0.7 Ma. The black stars are the location of the Amsterdam (Am) and St. Paul (SP) islands. The white dotted lines show the locations of the crustal cross section in Figure 4. (b) Topographic profile (black lines) and vertical lines showing the boundaries of multistage construction of the ASP Plateau (see white dotted line (2) above for location).

and 30 km long, respectively) that bracket a longer segment (I2, 100 km) around which most of the plateau has formed during the last 10 Myr (Figure 1). The ASP Plateau is presently in a period of diminishing plume-ridge interaction indicated by a decrease in axial crustal thickness since 1.4 Ma. Using high-resolution bathymetric (gridded at 200 m) and gravity data (gridded at 1 km) as well as magnetic anomalies from the PLURIEL (September/October 2006) and BOOMERANG 06 expeditions (February/April 1996; Maia et al., 2011; Scheirer et al., 2000), we present a detailed analysis of the Amsterdam-St. Paul Plateau and of the morphological evolution of the SEIR axis during the last 3 Myr. The observations at this scale reveal temporal variations in ridge-axis morphology and in crustal thickness perpendicular to, and along the axis of, the SEIR atop the ASP Plateau and reveal a complex interaction between the ASP plume and the ridge. To assess the role of along-axis variations in mantle source on the above observations, we use a combination of published geochemical data (Graham et al., 1999; Nicolaysen et al., 2007; Loewen et al., 2019; approximately 10-km sampling) and five new He isotopic analyses. With this combined data set, we review several hypotheses to explain each plateau characteristic. Comparisons of geochemical data with bathymetric and gravity data reveal that both the ASP plume and the ambient shallow upper mantle exert considerable influence on crustal production. Specifically, crustal thickness variations perpendicular to the ridge axis can be explained by recurring increases and decreases in the rate of plume upwelling, while

along-axis crustal variations may be governed by small-scale spatially distributed mantle heterogeneities in the upper mantle and in the plume.

## 2. The Amsterdam-St. Paul Plateau

The ASP Plateau straddles the SEIR, which separates the Australian plate to the northeast from the Antarctic plate to the southwest (Figure 1). The oldest portion of the plateau formed between 10 and ~3 Ma and is bounded by the Amsterdam and St. Paul fracture zones, respectively to the north and the south (Maia et al., 2011). Between SEIR segments H and I1, the Amsterdam transform fault (AFZ) defines the northern boundary of the younger portion of the plateau, whereas the overlapping and propagating ridge segments J1 and J2 define the southern boundary (Scheirer et al., 2000). Within the plateau, segments I1 and I2 are separated by a recently formed small discontinuity, the Boomerang transform (BTF; Scheirer et al., 2000). Segment I2 is composed of two parts: a northern short section (20 km long) and a southern, longer section (100 km long) that terminates in the south at the narrow Hillegom transform (HTF), the remaining active portion of the Saint Paul Fracture Zone (SPFZ; Conder et al., 2000). Our study focuses on the longer portion of the segment I2. Due to its anomalously thick crust (up to 12 km; Maia et al., 2011), negative mantle Bouguer gravity anomaly (Scheirer et al., 2000), and high  $^3\text{He}/^4\text{He}$  ratios up to 14 times the atmospheric value (~14 Ra; Graham et al., 1999; Nicolaysen et al., 2007), several authors propose a plume origin for the plateau (e.g., Graham et al., 1999; Johnson et al., 2000). However, the chemical and physical influence of the ASP plume only spans ~340 km along the SEIR (Graham et al., 1999), indicating a relatively small melting anomaly that is ~80 km in diameter (Maia et al., 2011).

Maia et al. (2011) conclude that the ASP Plateau had a multistage history that was dependent upon the interaction between the northeastward migrating SEIR (35 mm/year; Conder et al., 2000) and a variable flux mantle plume. Construction of the plateau occurred during stages of relatively high and relatively low axial magma flux. Stage A (~9.7–6.3 Ma) was associated with a high magma flux and corresponded to the early interaction of the plume and ridge. During this period, the plume center was NE of the SEIR and the plume-ridge distance progressively decreased while melt supply at the axis increased. The high magma fluxes yielded construction of a thick crust (~10 km) and smooth surface topography (Figure 1, Area A). Stage B began at 6.3 Ma with a southwestward jump of the ridge axis away from the ASP hot spot, which increased the plume-ridge distance and led to a decrease in the along-axis magmatic budget (Figure 1, Area B), as evidenced by thinner crust (~7 km). The lower axial magma flux coincided with deeper, rougher bathymetry and several V-shaped abyssal hills indicating along-axis propagation of changes in magma supply. Stage C began with a second southwestward ridge jump at 3 Ma (Figure 1, Area C), which caused the axis to nearly overlie the plume center. The ridge-centered plume initiated a second high magma flux period, strongly increasing the crustal thickness (~11 km). During this stage, the ridge migrated away from the plume center causing a decrease in magma supply as indicated by thinner crust (~8 km). Finally, stage D coincides with a modern, lower magma supply beginning 1.4 Ma (SE compartment) to 0.9 Ma (NW compartment). This lower magma supply has led to recent changes in faulting style of the ASP Plateau (Figure 1, Area D). Here, we focus on the role of the modern low-magma supply period on the evolution of the ASP Plateau since 3 Ma, including the recent rifting event.

## 3. Methodology

### 3.1. Geophysical Results

We use shipboard bathymetry and age derived from magnetic anomalies to calculate a residual bathymetry on the whole ASP Plateau (Figure 2). The magnetic anomaly was computed from the IGRF4505 model by Courtèges (2010). That study also provided detailed identification and interpretation of the magnetic anomalies. Residual bathymetry was calculated by subtracting the expected thermal subsidence of the seafloor (Parsons & Sclater, 1977) using a value of 342 m/Myr for the subsidence coefficient (Stein & Stein, 1992) and an average axial depth of 2,600 m from the original bathymetry. To calculate the Mantle Bouguer Anomaly, we subtract from the free-air anomaly the gravity effects of the seafloor-water (density contrast,  $\Delta\rho = 1,770 \text{ kg/m}^3$ ) and crust-mantle ( $\Delta\rho = 500 \text{ kg/m}^3$ ) interfaces assuming a constant crustal thickness of 6 km. The Residual Mantle Bouguer Anomaly (RMBA) is obtained after removal of the effect of lithosphere



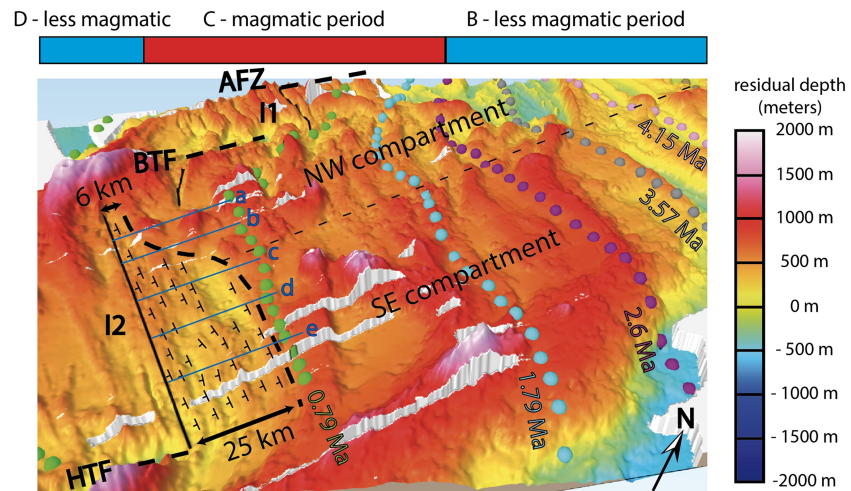


**Figure 2.** The 3-D residual bathymetry surface of the ASP Plateau viewed from the SE toward the NW. Most of the construction structure of the crust is readily discernible. The top horizontal scale shows the alternation between the magmatic (red blocks) and less-magmatic periods (blue blocks). From south to north, we can distinguish the Hillegom Transform Fault (HTF), segment I2, segment I1, and the Amsterdam Fracture Zone (AFZ). Long dashes with ticks represent strike and dip of normal faults bounding abyssal hills during the rifting period. The color circles identify magnetic anomalies. The transition from more robust magmatic construction (Area C) to rifting (Area D) is represented by the thick black dash line, which also marks a change from large abyssal hill fabric to much smaller hills. Thin black dashed line mark the separation between the NW and SE compartment. Thin blue lines mark the location of the topographic profiles shown in Figure 3 and white areas represent missing ship coverage.

cooling using an age grid as in Maia et al. (2011) and is then inverted for variations in crustal thickness assuming a constant density in both crust and mantle (e.g., Kuo & Forsyth, 1988).

### 3.2 Helium Isotope Analyses

Five basalt samples along the present day ridge axis in the study area were analyzed for  $^3\text{He}/^4\text{He}$  and vesicle [He] to supplement the existing helium isotope data from Graham et al. (1999) and Nicolaysen et al. (2007). The samples were recovered by the Boomerang 06 expedition, and include two fresh basalts from the axial valley of segment I2 (D65 and WC36), a basalt from segment J1 (WC32), and two aphyric pillow basalts from the axial valley of segment J2 (D50 and WC23). Large chips of glass were crushed to several millimeters in size and the freshest material was hand picked using a binocular microscope to avoid visible oxidation and alteration. The chips were ultrasonically cleaned in deionized water followed by acetone, and air dried. The samples were then placed in an ultrahigh-vacuum crusher for helium measurements, and crushed 75 times using a magnetic piston actuated by external solenoids. Sample weights ranged between 130 and 215 mg. The samples were analyzed at Oregon State University following procedures described in Graham et al. (2014). The results were compiled with previous  $^3\text{He}/^4\text{He}$ , K/Ti and  $\text{Na}_8$  on-axis data from Graham et al. (1999), Douglas-Priebe (1998), and Nicolaysen et al. (2007).  $\text{H}_2\text{O}/\text{Ce}$  ratios are from Loewen et al. (2019), and  $\Delta 8/4$  following Hart (1984) was computed from the Pb isotope data of Nicolaysen et al. (2007). The compiled results are reported in Tables S1 and S2 in the supporting information.

Some older to zero age samples are available (WC45, WC44, WC34, D58-1, D58-4, and D24) and could be useful in order to better constrain the evolution of the geochemical sources through time. This statement is true only if samples reflect the lithosphere at the time when they built or if geochronological are available. Sample D24 is a dredge rock collected from a seamount and was dated at  $\sim 5$  Ma (Janin et al., 2011) but is emplaced on a younger age crust. So according to Janin et al. (2011) this age is false and cannot be linked to geophysical observations. The remaining five other samples sit on the south to the ridge portion of the plateau (WC45, WC44, WC34, D58-1, D58-4), where off-axis seamounts overprint magnetic anomalies of the lithosphere. In the absence of age calibration of those specific samples, it is very delicate to discuss the significance of their geochemical composition relative to geophysical observations and to evolution of the plateau. Therefore, we chose to be cautious and not include these samples in the present study.

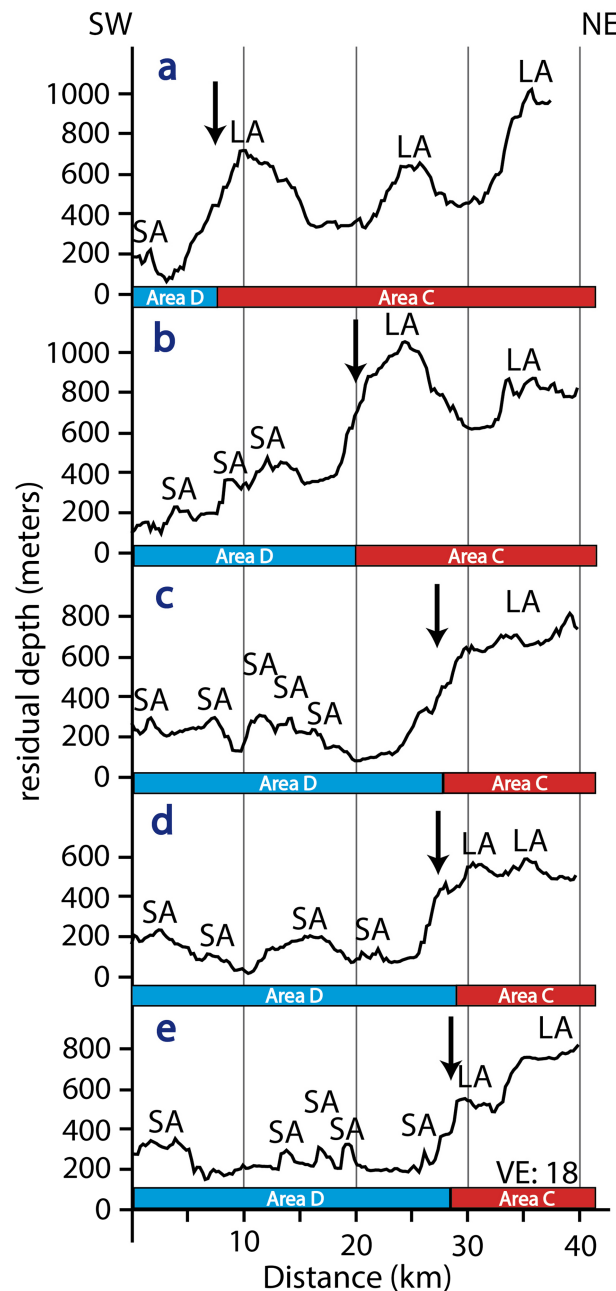


**Figure 3.** Residual depth profiles showing the morphological structure of the ASP Plateau since ~1.5 Ma (see blue thin lines in Figure 2 for cross-section locations). An abrupt change in the bathymetric expression of rifting (thick black arrows, the transition from stage C to stage D marked by the red/blue color bar) is preceded by large abyssal hills associated with higher magma fluxes (LA) and followed by several small abyssal hills (SA). Vertical Exaggeration (VE) = 18.

#### 4. Geometry, Morphology, and Inner Structure of the ASP Plateau

Structural analyses and cross sections (Figure 3) from our new map of residual bathymetry (Figure 2) provide important constraints on the evolution of the ASP Plateau and its recent change in rifting behavior. The stage C (Area C) displays a regularly spaced abyssal hill fabric parallel to both magnetic anomalies and the current ridge axis (N145°E). The southern portion of Area C hosts abyssal hills (Figure 3; “LA”) up to 300 m high, 4 to 7 km wide in the across axis direction, and separated by short sections of flat topography. The northern part of Area C hosts abyssal hills up to 400 m high, 5 to 10 km wide, and oriented oblique to the strike of the SEIR.

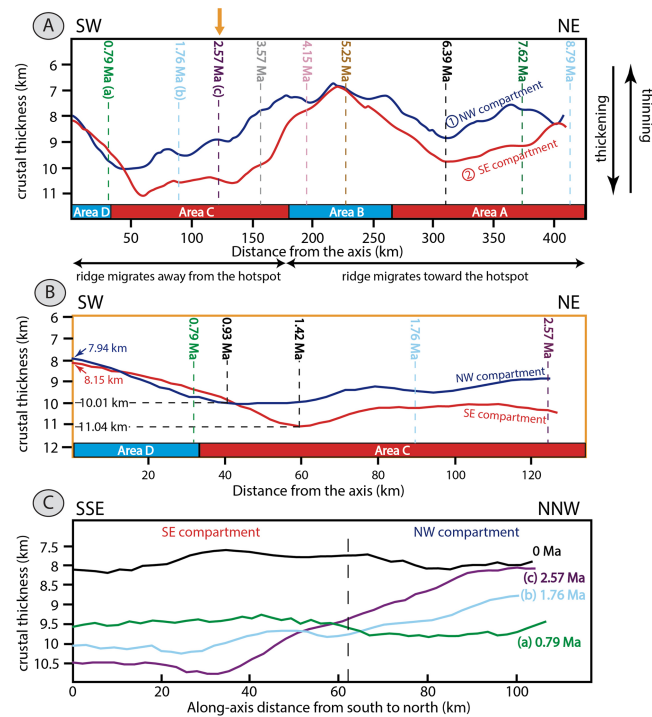


**Figure 4.** Crustal cross section perpendicular to the ridge axis across the NW compartment (blue line) and across the SE compartment (red line) during (a) the last 9 Myr and (b) the last 2.5 Ma. Orange arrow indicate the end x axis of (b). Horizontal scale shows the alternation between the magmatic (red block) and less-magmatic periods (blue block) defined from residual topography by Maia et al. (2011). Colored vertical lines indicate the location of the magnetic anomalies. (c) Along-axis crustal thickness variation at 0, 0.79, 1.76, and 2.57 Ma.

The associated graben displays a similar variation in orientation reflecting abandoned spreading segments corresponding to aborted propagation (Deschamps et al., 2008). The transition between axis parallel to axis oblique abyssal hills from south to north is diffuse and marked by the presence of punctuated off-axis small volcanoes. These volcanoes define a line across the plateau (Figure 1), perpendicular to the segment I2 axis, that separates the plateau into two structurally distinct compartments: the NW and the SE compartment (Figures 1, 2, and S1 in the supporting information; Maia et al., 2011). Structural variations between compartments are also observed at the transition between the stage C and stage D (Areas C and D).

The transition from the stage C to stage D is marked by an abrupt break in the bathymetry as indicated by a sudden deepening of the seafloor by ~500 m (Figure 3). The bathymetric break is farther from the ridge axis in the SE compartment (~25 km) than in the NW compartment (~6 km) and corresponds to a change in the style of rifting of the plateau. This change in rifting style (stage D) occurs earlier in the SE compartment (~0.7 Ma) than in the NW compartment (~0.1 Ma). The shape of the rifting boundary is sigmoidal with the boundary roughly following the ridge axis until undergoing a sudden S-shaped curve at the diffuse boundary between the two compartments (Figure 2). To the southwest of the break in bathymetry, the deeper, rougher bathymetry is characterized by a succession of small, regularly spaced abyssal hills (Figure 3, “A”; 30–100 m high and 2–5 km wide) and grabens. The abyssal hills strike parallel to the ridge axis and extend to the north from 0.7 to 0.1 Ma. Since the last 0.1 Ma, abyssal hills strike parallel to the ridge and occur along the complete I2 segment of the SEIR.

The structural architecture of the crust is further constrained by variations in gravity-derived crustal thickness (Figure 4). Cross sections perpendicular to the ridge axis show that periods of positive relative depth anomalies correspond to periods of relatively thick crust between 8–6 and 1–3 Ma (Figure 4a). Together, these observations indicate two periods of strong magmatic activity along the SEIR axis corresponding to Areas A and C and separated by Area B, where negative depth anomalies and relatively thin crust suggest a decreased magma supply (Maia et al., 2011). The transition between the earlier highly magmatic and

less magmatic stages (Stage A to Stage B) is marked by decreases in crustal thickness. The decrease starts synchronously in the NW and SE compartments at  $\sim 6.39$  Ma. During highly magmatic stages (Stages A and C), crustal thickness in the NW and SE compartments reach up to 8.75 and 10 km, respectively, in Area A, and up to 10 and 11 km, respectively, in Area C, with crustal thickness being generally less in Area A than in Area C (Maia et al., 2011). Moreover, over the last 9 Myr the SE compartment of the spreading segment I2 displays thicker crust and shallower depths than the NW compartment except around 5 Ma.

Since 3 Ma, gravity-derived crustal thicknesses increased and then decreased prior to the most recent change in faulting style of the ASP Plateau (Area D; Figure 4b). Crustal thickness began decreasing in Stage D, but this occurred earlier in the SE ( $\sim 1.42$  Ma) than in the NW ( $\sim 0.93$  Ma). The sudden deepening in residual bathymetry and decrease of crustal thickness suggest a reduced supply of melt along the ridge axis and mark the transition from a highly magmatic stage to the current, more rifting dominated stage. The onset of reduced magma supply in the south happened at 1.42 Ma, while melt production remained high in the north until 0.93 Ma. Since 0.93 Ma, crustal thickness in the NW and SE compartments has been comparable ( $\sim 10$  km) and diminished with a similar rate, and the distinction between both compartments is no longer significant. Together, along-axis crustal thicknesses and residual depths suggest that changes to the basal topography of the crust through time were modulated by changes in axial melt production. Between 2.57 and 1.76 Ma, the crust was thicker in the SE than in the NW compartment. This gradient in crustal thickness can be interpreted as a basal crustal slope, and results in an average basal northern upslope estimated between  $2.2^\circ$  and  $1.3^\circ$ . The angle of the basal slope decreased over time, seemed to reverse at 0.79 Ma, and is absent beneath the present-day axis (Figure 4c).

For comparison, the segments outside the study area (H to the north, and J1 and J2 to the south), show current residual depth and gravity-derived crustal thicknesses that are somewhat greater than expected for spreading ridges having no hot spot influence (e.g., Schilling, 1991). Segment H is characterized by average residual depths of  $-560$  m but it has a normal crustal thickness of 6 km. Segments J1 and J2 are characterized by average residual depths of  $-100$  to  $200$  m and crustal thickness of 7–8 km. However, comparable off-axis surveys are not available in the H and J1, J2 regions to provide a temporal resolution similar to what is available in the I1 and I2 tectonic corridors of this study.

## 5. Ridge, Plume, and Mantle Source Control on the Development of the Plateau

The residual bathymetric observations and gravity-derived crustal thickness indicate that the 3-D morphological architecture of the plateau is controlled by differences in melt production. The timing and intensity of volcanism due to plume-ridge interaction evolved both temporally and spatially, leading to variations in melt production that were both perpendicular and parallel to the ridge axis. Thus, the following questions arise: (1) what factors control the morphology of the ASP Plateau and the variation in strength of the plume-ridge interaction? (2) How did the morphology of the plateau evolve relative to mantle upwelling rate, the geometry of the ridge axis, and the distance between the plume and the ridge? (3) What are the roles of spatial and temporal differences in mantle source composition? (4) Are the above factors capable of producing the observed changes in crustal thickness both perpendicular and parallel to the ridge axis? In the next sections, we will attempt to answer these questions and discuss processes that may influence the evolution of the melt production at the ridge axis.

### 5.1. Variation in Melt Production Through Time

Geophysical data presented in this paper are consistent with the formation of the ASP Plateau as resulting from the interaction between the ASP plume and the SEIR. The ASP plume provided excess melt that produced anomalous bathymetry and excess crust (Zhao, 2007). The temporal changes in crustal thickness suggest a variable rate of plume upwelling, which would yield changes in melt production at the ridge axis. Possible causes for such temporal variations in the plume upwelling rate include the balance between the tectonic extension and magmatic accretion (Buck et al., 2005), or long-period (e.g.,  $\sim 3$ – $20$  Myr) oscillations in the plume conduit (Whitehead, 1982). Additionally, over a plume/ridge interaction period of  $\sim 10$  Myr, the relative motion (direction and velocity) and the distance between the spreading ridge and the plume center may also influence the rate of melt production (e.g., Ito et al., 1997; Ribe & Delattre, 1998).

The ASP Plateau is characterized by highly variable seafloor morphologies marked by a succession of abyssal hills and grabens (Maia et al., 2011). The development of an axial high (i.e., hills) or axial valley (i.e., grabens) depends on lithosphere temperature and on melt availability (e.g., Chen & Lin, 2004) and also on the rate of dyking relative to tectonic extension (Ito & Behn, 2008), which will be influenced by variations in plume upwelling rate. Indeed, numerical models that simulate a robust melt supply by frequent dike injections that accommodate plate separation, and low-melt supplies that accommodate plate separation tectonically by passive stretching and faulting of the lithosphere, suggest that magmatic accretion is a strong control on axial morphology (Behn & Ito, 2008; Buck et al., 2005). The models are quantified primarily by using a ratio of magmatic to tectonic axial accretion ( $M$ ). In terms of mechanical deformation, recent analogue modelling indicates the predominant behavior of axial lithosphere during failure is either brittle or plastic (Sibrant et al., 2018). This deformation behavior is described by the axial failure parameter ( $\pi_F$ ): plastic failure occurs at magmatically robust conditions involving dike intrusion, while brittle failure occurs at magmatically poor ridges where faulting dominates. A change from robust magmatism associated with large volcanic highs to a more faulted terrain with small abyssal hills as magma supply diminishes is consistent with a decrease in " $M$ " (less magmatically robust) and increase in " $\pi_F$ " (thick elastic axial lithosphere) as observed in the Azores (Cannat et al., 1999). For the recent evolution of the ASP Plateau, crustal thickness began decreasing at  $\sim 1.42$  and at  $\sim 0.93$  Ma, in the SE and NW compartments (Figure 4b), while the topographic transition between the magmatic stage C and the less magmatic stage D occurred at  $\sim 0.7$  Ma and  $\sim 0.1$  Myr. This suggests that the shift in axial deformation from more plastic with fewer faults (low " $\pi_F$ ", high " $M$ ") to more brittle with larger faults (higher " $\pi_F$ ", lower " $M$ ") required  $\sim 700$  kyr.

At a larger scale, during the last 10 Myr the two periods of increased melt supply (Stage A and Stage C) are separated by a low magmatic phase over a time span of  $\sim 3$  Myr (Stage B). Temporal variation in plume upwelling has been suggested for several plumes, such as Hawaii, Tristan da Cunha, and Iceland (Adam et al., 2007; Hanan & Schilling, 1997; Ito, 2001; Schilling & Noe-Nygaard, 1974; Weiss et al., 2016). Such "plume pulses" may occur with regular recurrence periods that differ between plume localities. Investigations of conduit dynamics show that under some conditions, which may prevail in the mantle, plumes are neither steady nor uniform (Scott et al., 1986; Whitehead, 1982). A variety of buoyancy-driven instabilities could disrupt continuous conduits into arrays of discrete diapirs or blobs. These instabilities could be caused by bending of the conduit by more than  $60^\circ$  (Whitehead, 1982) due to large-scale mantle circulation (Olson & Singer, 1985; Steinberger, 2000). Such instabilities are predicted to occur over relatively long periods of 10–20 Myr, although recent numerical simulations suggest that inclusion of appropriate mantle rheological behavior can result in shorter periods ( $\sim 3$ –8 Myr; Neuhaert & Mittelstaedt, 2017). In addition, unsteady behavior is observed within experimental plume conduits, in the form of vertically propagating variations of conduit diameter and discharge (Maiden & Hoefer, 2016; Schubert et al., 1989; Scott et al., 1986). These disturbances occur as large-amplitude solitary waves with an oscillation period of 3 to 6 Myr (Adam et al., 2007). Those oscillations may also induce geochemical variations in Pb isotopes (e.g., Iceland; Hanan & Schilling, 1997) and rare earth elements contents (e.g., Faeroe Islands; Schilling & Noe-Nygaard, 1974). A period of  $\sim 3$  Myr is consistent with the duration of Stage B on the ASP Plateau and corresponds to temporally varying magma flux predicted by laboratory and numerical modelling. Therefore, the  $\sim 3$ -Myr oscillations observed in the construction of the ASP Plateau could correspond to variations in the ASP plume flux, as previously suggested by Maia et al. (2011).

Bathymetry and gravity-derived crustal thickness also indicate that the crust is thinner during Stage A (Area A) than Stage C (Area C; Figures 1 and 4). This difference may reflect the increased plume-ridge separation during formation of Area A than during formation of Area C. Results of numerical models indicate that ridge migration relative to a plume can affect the duration and the strength of the connection to the ridge. Indeed, maximum interaction distance is predicted to be higher for a ridge receding from a plume than for a ridge approaching a plume (Ito et al., 1997; Ribe & Delattre, 1998; Schilling, 1985). Studies of the interaction between the Foundation Seamounts mantle plume and the Pacific-Antarctic ridge where the ridge is currently approaching the plume confirm the model results (Maia et al., 2000, 2001). Consequently, for a given plume-ridge distance, the connection is stronger (i.e., more plume material reaches the axis) when the ridge is migrating away from the plume and this will generate a thicker crust. Plate reconstructions suggest that the ASP plume was ridge-centered at  $\sim 4$  Ma (Maia et al., 2011). During Stage C from 3.75 to 1 Ma, the distance between the hot spot and the ridge increased, forming a thicker crust than during Stage A (from



9 to 6.3 Ma), which was a period when the ridge was moving toward the plume (Maia et al., 2011). From this observation, it seems reasonable to infer that the difference in crustal thickness between these two periods of construction reflects how the SEIR was migrating relative to the ASP plume.

To summarize, we propose that the variation of the melt production through time (i.e., perpendicular to the ridge axis) was controlled by periodicity in plume upwelling coupled with changing plume-ridge distance. However, these do not account for the observed variations in along-axis crustal thickness and morphology. Indeed, plate reconstructions indicate that ridge migration was perpendicular to the axis direction, and interaction with the plume's central axis was along segment I2 (Figure 1; Maia et al., 2011). The plume center was at an equal distance from both I2 compartments (61 and 58 km), and thus, variation in plume upwelling should have shown a similar strength along the entire segment I2. The distinct compartmentalization and particularly the progressive northward rifting may relate to an intrinsic characteristic such as tectonic segmentation of the ridge (e.g., Carbotte et al., 2004), or to along-axis differences in melt transport (Braun & Sohn, 2003; Magde & Sparks, 1997), both of which would depend on the architecture of the lithosphere. Alternatively, the compartmentalization may result from compositional/lithologic heterogeneities in either the plume, the upper mantle, or both (e.g., Cushman et al., 2004; Nicolaysen et al., 2007; Schilling et al., 1982, 1983).

## 5.2. Along-Axis Variation of Melt Production

Differences in melt production along the ridge axis (i.e., parallel to the magnetic anomalies) have been variable through time and separate segment I2 into two compartments. During the robust magmatic stages, abyssal hills are larger and the crust is thicker in the SE than in the NW. Moreover, the most recent stage of low-magma supply began earlier in the SE (~1.47 Ma) than in the NW (~0.93 Ma). This last observation is particularly enigmatic and the following section discusses several possible hypotheses to explain this difference in melt supply along segment I2.

The above distinctions between crustal compartments may have been caused by recent reorganization in the geometry of the SEIR. Previous studies suggest that the progressive south to north change in faulting style of the ASP Plateau during the last 1 Myr was induced by a ridge instability, such as a ~90-km ridge jump (Conder et al., 2000) or ridge propagation of the I2 SEIR segment (Maia et al., 2011). A ridge jump would be inferred from a blending in age of the magnetic anomalies, while ridge propagation would be seen in the progressive increase of the length of the magnetic anomalies through time. Both types of ridge instability have been suggested based on irregular magnetic anomaly patterns, and have been observed along plume-affected ridges such as the intermediate spreading Galápagos Spreading Center close to the Galápagos hot spot (Hey et al., 1977; Hey & Vogt, 1977; Mittelstaedt et al., 2012), and along the slow spreading southern Mid-Atlantic ridge at 9°S near Ascension Island and at 16°S near St. Helena (Brozena & White, 1990). However, the regular decrease in age of magnetic anomalies on the ASP Plateau toward the axis, and their quasi constant geometry indicates that the current pattern of segmentation along this portion of the SEIR has remained stable since ~3.6 Ma (Figures 2 and S1).

### 5.2.1. Influence of Subaxial Lithosphere Structure on Crustal Accretion

It has been suggested that melt can be collected at an impermeable boundary at the top of the melting column and then migrate laterally along this sloping boundary toward the ridge (Sparks et al., 1994; Sparks & Parmentier, 1991). Moreover, 3-D numerical models predict that ridge segmentation can induce melt focusing not only toward but also along the axis (e.g., Hebert & Montési, 2011). For example, at the slow-spreading Mid-Atlantic Ridge, Magde and Sparks (1997) argued that melt migration along a permeability barrier generates more realistic variations in crustal thickness than diapiric instabilities. This permeability barrier is believed to form at the top of the melting column by a multisaturation point of plagioclase and pyroxene (Montési et al., 2011). Following this idea, plume melts could migrate buoyantly beneath the ridge axis until reaching the shallowest part of the axial lithosphere.

Here, we first consider a model where the crustal thickness depends only on mantle temperature (Klein & Langmuir, 1987) and that the thermal anomaly also corresponds to a change in lithosphere thickness. Along segment I2 between 2.57 and 1.76 Ma, the crust is thicker in the SE ( $11 \pm 0.6$  km) than in the NW compartment ( $10 \pm 0.4$  km) resulting in a basal northern upslope that is between 2.2° and 1.3°. Based upon the evolution in crustal thicknesses, the angle of the basal slope decreased over time, reversed at 0.79 Ma, and is absent beneath the present-day axis (Figure 4c). Assuming a uniform distribution of fertile plume material

beneath the axis, the crustal thickness difference between the SE and NW compartments requires an ambient mantle temperature difference between the compartments of  $\sim 30^\circ\text{C}$  to  $\sim 50^\circ\text{C}$  at  $\sim 2.57\text{ Ma}$ , depending on the model used (Chen, 1996; McKenzie, 1984). This thermal difference can be converted to an axial lithospheric thickness difference using a 1-D advection-diffusion solution (Mjelde et al., 2008) with a thermal diffusivity of  $\kappa = 10^{-6}\text{ m}^2/\text{s}$  (Turcotte & Schubert, 2002); and considering that the mantle rises under the axis with a velocity equal to the half-spreading rate  $V/2$  (with  $V = 65\text{ mm/year}$ ). The axial lithospheric thickness can be estimated by

$$Z_{\text{axis}} = -\frac{2\kappa}{V} \log\left(\frac{T_c - T_m}{T_0 - T_m}\right),$$

where  $T_m = 1,470^\circ\text{C}$  is the ambient mantle temperature (Dalton et al., 2014),  $T_0 = 0^\circ\text{C}$  is the surface temperature, and  $T_c = 650^\circ\text{C}$  is the assumed temperature of the brittle-ductile transition. The difference in lithospheric thickness ( $\Delta Z$ ) between the SE and the NW compartments estimated using the above mantle temperature difference ( $T_m + \Delta T$ ) is between 4 and 11 m, resulting in a basal southern upslope that is only between  $0.003^\circ$  and  $0.009^\circ$ .

Along segment I2, the shallowest part of the lithosphere corresponds to a thicker crustal compartment, that is, the SW compartment. Based upon the above considerations, we suggest that it is unlikely that thermal anomalies or lithospheric slopes along the I2 segment can explain a crustal thickness variation of 1 km. The lithospheric thickness variations and slopes estimated from the equation of Mjelde et al. (2008) correspond to an upper bound, since changes in the composition of the mantle as well as isostatic compensation were not taken into consideration.

### 5.2.2. Variable Influence of the Amsterdam-St. Paul Mantle Plume Along the SEIR

Differences in melt supply between the NW and SE compartments on the plateau could potentially result from local variability in the ASP plume at the ridge segment scale or less ( $\sim 10\text{--}100\text{ km}$ ; e.g., Schilling, 1991; Cannat et al., 1999; Chen & Lin, 2004). Plume influence and strength can be tracked through the amplitude of physical and chemical anomalies along the spreading ridge. For example, the presence of elevated ratios of  $^3\text{He}/^4\text{He}$  and incompatible elements such as  $\text{K}/\text{Ti}$  are believed to be reliable indicators of enriched plume material (Kurz et al., 1982; Lupton, 1983). Basalts along segment I2 show a peak in both of these ratios at the transition between the NW and SE compartments (Figure 5). Higher  $^3\text{He}/^4\text{He}$  ( $11.1\text{--}12.2\text{ R}_A$ ) and  $\text{K}/\text{Ti}$  ( $0.51\text{--}0.61$ ) ratios are present at the center of the I2 segment while lower  $^3\text{He}/^4\text{He}$  ( $8\text{--}9.5\text{ R}_A$ ) and  $\text{K}/\text{Ti}$  ( $0.2\text{--}0.3$ ) ratios are present along segments I1, J1, and J2 outside the main part of the ASP Plateau. In contrast, and somewhat surprisingly,  $^3\text{He}/^4\text{He}$  ratios extend to higher values ( $14\text{ R}_A$ ) along segment H immediately to the north of the plateau. This elevated  $^3\text{He}/^4\text{He}$  anomaly was attributed to pollution of the subridge mantle beneath segment H by distal, cooler portions of the plume that were less depleted by melting, compared to the core of the plume, centered beneath the plateau and influencing segment I2 (Graham et al., 1999). The peak in  $^3\text{He}/^4\text{He}$  and  $\text{K}/\text{Ti}$  at the transition between the NW and SE compartments, therefore, seems to correspond to the location of the strongest plume influence along the SEIR axis.

In Figure 5, the peak in  $^3\text{He}/^4\text{He}$  at the transition between the compartments does not correspond to a peak in crustal thickness. Indeed, the crustal thickness in the NW and SE compartments is effectively the same ( $\sim 8\text{ km}$ ). This observation indicates that the ASP plume may be weaker at present than in the past and may be incapable of producing large crustal anomaly differences near the center of the ASP plume. This assumption can be further tested using basalt  $\text{Na}_8$  contents (Figure 5). Assuming a relatively uniform  $\text{Na}$  concentration in the underlying mantle peridotite (Klein & Langmuir, 1987; Langmuir et al., 1992), a higher  $\text{Na}_8$  content in basalt reflects a smaller extent of melting (from cooler mantle), while lower  $\text{Na}_8$  reflects a larger extent of melting (from warmer mantle). The  $\text{Na}_8$  contents of zero-age basalts erupted along segments I1, I2, and J1 atop the ASP Plateau show considerable variability, and are not correlated with the crustal thickness variation (Figure 5). The most obvious feature is a transition from lower values along segment I2 to higher values along segment J1. This abrupt transition is inconsistent with the comparable crustal thicknesses between SW-I2 and J1 segments. However, the transition is consistent with larger extents of melting along segment I2 compared to segments J1 and J2. Within segment I2 itself the  $\text{Na}_8$  values are variable and appear to show a weak gradient from higher values in the NW to lower values in the SE (Figure 5). The lowest  $\text{Na}_8$  along I2

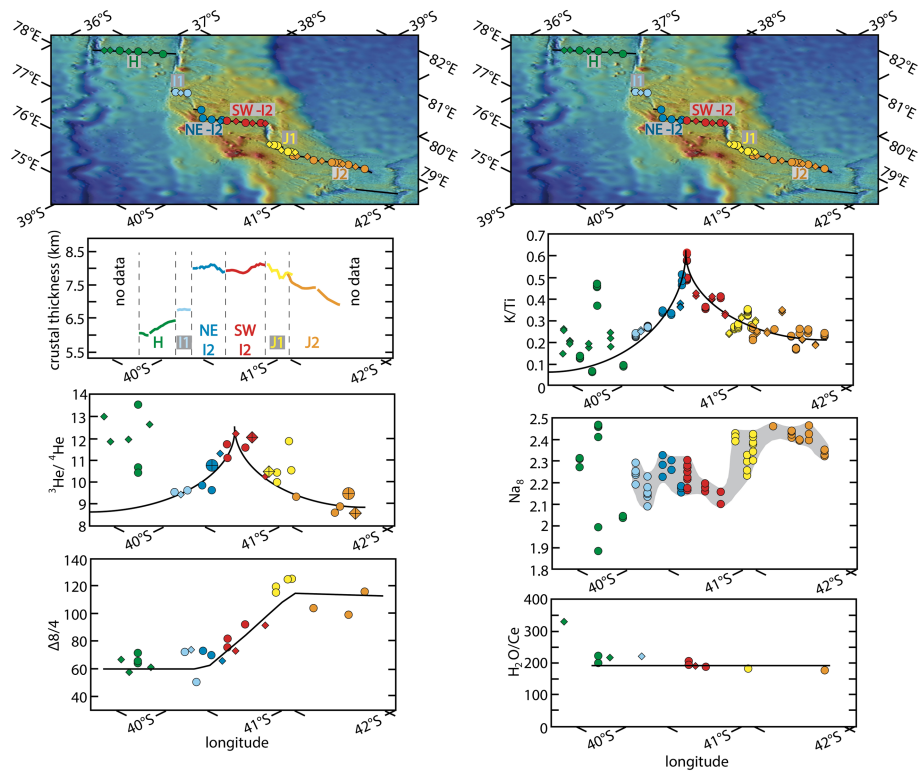


**Figure 5.** Along-axis geochemical and crustal thickness variations. Bathymetric map (GeoMapApp) is included at the same scale to show ridge features and locations of basalts. The  $^3\text{He}/^4\text{He}$  ( $R/R_A$ ),  $\text{K}/\text{Ti}$ , and  $\text{Na}_8$  data are taken from Graham et al. (1999) and new results of this study,  $\text{H}_2\text{O}/\text{Ce}$  ratios are from Loewen et al. (2019), and  $\Delta 8/4$  has been calculated from the Pb isotope data of Nicolaysen et al. (2007).  $\text{Na}_8$  is the crystal fractionation adjusted composition of  $\text{Na}_2\text{O}$  following Klein and Langmuir (1987). Circles indicate dredges and diamonds are wax cores. Symbols with crosses inside correspond to new helium data (this study). The black lines and grey area schematically depict the main tendencies for axial lavas.

does not occur in basalts with the highest  $\text{K}/\text{Ti}$  and  $^3\text{He}/^4\text{He}$  ratios, where the plume influence is postulated to be greatest. Also, the highest  $^3\text{He}/^4\text{He}$  and  $\text{K}/\text{Ti}$  ratios along segment I2 are not accompanied by a thick zero-age crust (Figure 4c). Both crustal thickness and  $\text{Na}_8$  indicate that the peaks in  $^3\text{He}/^4\text{He}$  and  $\text{K}/\text{Ti}$  do not necessarily correspond to an increase in the extent of partial melting related to an increase in mantle temperature, but instead may be a localized feature marking an increased contribution from distinct/heterogeneous plume material to the subridge mantle beneath segment I2. Such interspersed features may also account for variability of the ratios measured within each area. For example, the NW compartment shows  $\text{K}/\text{Ti}$  ratios between 0.3 and 0.5. Furthermore, in conjunction with the  $^3\text{He}/^4\text{He}$  variations, the hydrogen isotope compositions ( $\delta\text{D}$ ) of ASP basalts suggest that the ASP plume contains a mixture of recycled lithospheric material and primordial mantle (Loewen et al., 2019). Altogether, the variability in  $^3\text{He}/^4\text{He}$ ,  $\text{K}/\text{Ti}$ , and  $\delta\text{D}$  of ASP basalts appears to indicate significant spatial heterogeneity in plume composition, or in the plume contribution to axial magmatism over short distances (1–10 km).

Based upon the above geochemical data we suggest that the ASP plume is small (i.e., less than 80 km in diameter), and relatively weak at the present time, with a variable contribution to magmatism along segment I2 and possibly heterogeneous in composition (primordial mantle with additional recycled lithosphere; Loewen et al., 2019). The observed structural differences between the SE and NW compartments have remained steady since 10 Ma. We conclude that changes in plume upwelling contributed to the differences in crustal architecture (e.g., during the high and low magmatic periods), but an additional factor, discussed below, may also be involved to fully explain the observed characteristics of the ASP Plateau.

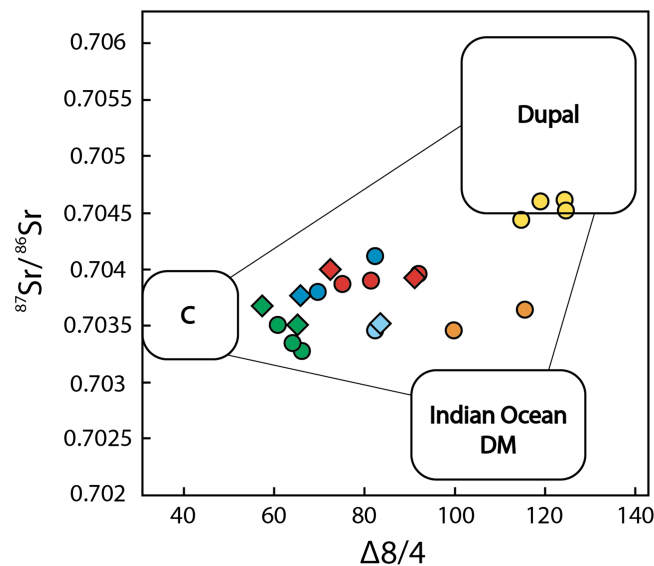


**Figure 6.** The  $^{87}\text{Sr}/^{86}\text{Sr}$  versus  $\Delta 8/4\text{Pb}$  for the Southeast Indian Ridge along the ASP Plateau. Note that basalt from segment I2, I1, and H tend to be offset toward relatively lower  $\Delta 8/4\text{Pb}$  compared to segments J1 and J2. Three mantle components are depicted: the common mantle component C (Hanan & Graham, 1996), DUPAL-type material, and depleted Indian MORB mantle (DM). The  $^{87}\text{Sr}/^{86}\text{Sr}$  data are from Nicolaysen et al. (2007). Symbols and colors as for Figure 5.

### 5.2.3. Influence of Mantle Source Variation on Crustal Accretion

The observed differences between the SE and NW compartments may include the effects of a variable mantle source, related to compositional/lithologic heterogeneity in either the plume, the upper mantle, or both. Radiogenic isotope ratios in young basalts provide a record of isotopic variations in the underlying mantle that originate from long-term differences in parent/daughter ratios (White & Schilling, 1978). Due to elemental fractionation in ancient melting events and tectonic recycling of lithosphere and crust, the parent/daughter ratios can be distinct in lithologically different materials such as peridotite and pyroxenite (e.g., Hirschmann & Stolper, 1996). One useful parameter in this regard is  $8/4\text{Pb}$ , defined as the vertical deviation from a Northern Hemisphere Reference Line (NHRL) by Hart (1984), where  $8/4\text{Pb} = [(^{208}\text{Pb}/^{204}\text{Pb})_{\text{sample}} - (^{208}\text{Pb}/^{204}\text{Pb})_{\text{NHRL}}] \times 100$ , with the NHRL equation being  $^{208}\text{Pb}/^{204}\text{Pb} = 1.209 (^{206}\text{Pb}/^{204}\text{Pb}) + 15.627$ . Using Pb isotope variations measured in young SEIR basalts by Nicolaysen et al. (2007), we note that  $8/4\text{Pb}$  in basalts from segments J1 and J2 have a relatively high value ( $\sim 110$ ; Figure 5) consistent with a strong contribution from the Dupal anomaly (Dupré & Allègre, 1983). In contrast, basalts from segment H and I1 have lower  $\Delta 8/4\text{Pb}$  values ( $\sim 60$ ) that appear to be a mixture of a mantle component commonly found in mantle plumes (the component C of Hanan and Graham (1996)) with the depleted, shallow upper mantle underlying the SEIR. The central segment I2 (100 km in length) shows intermediate values of  $\Delta 8/4\text{Pb}$ , and ranges between 70 and 80 (i.e., variation of  $\Delta 8/4\text{Pb}$  about  $\sim 20$ ; Figure 5). This three-component mixing model for SEIR basalts is also supported by the Sr isotopic data. In the  $^{87}\text{Sr}/^{86}\text{Sr}$  versus  $\Delta 8/4\text{Pb}$  plot (Figure 6), basalts from ASP segment J1 and J2 define a trend between depleted, Indian Ocean upper mantle (DM), and enriched Dupal component. In contrast, basalts from ASP segments I2 (SE and NW compartments), I1 and H show lower  $\Delta 8/4\text{Pb}$  for a given  $^{87}\text{Sr}/^{86}\text{Sr}$ . There is a progressive decrease in  $\Delta 8/4\text{Pb}$  northward, suggesting an increasing contribution of the mantle component C from segment J2 to H. This increased northward C contribution is not correlated with a northward increase in crustal thickness (i.e., from J2 to H; Figure 5).

The Pb isotope variability could be related either to isotopic variations in either the ASP plume or in the upper mantle. The presence of high  $^3\text{He}/^4\text{He}$  ratios along segment I2 suggests that the ASP mantle plume is derived from a high  $^3\text{He}/^4\text{He}$  source region. This plume mantle source has  $^3\text{He}/^4\text{He}$  ratios significantly higher than the shallow Indian Ocean MORB mantle ( $^3\text{He}/^4\text{He} = 7 - 10 \text{ Ra}$ ; Graham et al., 2014). Hot spots having high  $^3\text{He}/^4\text{He}$  ratios are generally taken to be sourced at significantly greater depths than the MORB

mantle source (Kurz et al., 1982). This assumption is supported by whole-mantle tomographic images which indicate a core-mantle boundary source for the Amsterdam-St. Paul plume (Zhao, 2007). Nevertheless, the K/Ti and  $^3\text{He}/^4\text{He}$  peaks are relatively symmetric atop the plateau along segments I1, I2, and J1, while there is a gradient in  $\Delta 8/4\text{Pb}$ . This contrast suggests that the variation in  $\Delta 8/4\text{Pb}$  is not solely related to differences in plume influence but is also related to intrinsic Pb isotope variability in the ambient upper mantle. An enriched (Dupal) component is likely dispersed in the ambient upper mantle, as noted by Nicolaysen et al. (2007), and it may be stronger beneath the SE compartment of the ASP Plateau.

Outside the plateau and in its northern border, geophysical and geochemical data indicate that segments H and I1 are characterized by relatively deep residual bathymetry and normal (6–7 km) crustal thicknesses, and a stronger contribution from the mantle component C. In contrast, in the southern part of the plateau, segments J1 and J2 are characterized by shallow residual bathymetry and thicker crust (7–8 km), and a stronger Dupal component contribution. This suggests that, in the neighborhood of the ASP plume, the presence of the Dupal component may contribute to a thicker crustal production. Therefore, during the most recent and less robust magmatic Stage D (Area D), the ASP plume has been weaker in its melt supply, and shallow mantle source variations have been more influential in the variable melt production between the segments. Indeed, the difference in  $\Delta 8/4\text{Pb}$  of  $\sim 50$  between the northern and the southern boundary of the ASP Plateau seems to covary with crustal thickness variations of up to 1.5 km. Thicker crust correlates with higher contributions from the Dupal component, suggesting that the Dupal component may contain a more fertile lithologic heterogeneity such as garnet pyroxenite or eclogite. Variable contributions from the different mantle sources have led to variations in melt production that are consistent with the long-term thicker crust in the SE plateau compartment compared to the NW compartment.

At the present time there is no discernible variation in crustal thickness or residual bathymetry along the ridge axis of segment I2 (Figures 2–4). Moreover, the zero-age basalts show a small variation of  $\Delta 8/4\text{Pb}$  of about  $\sim 20$  along I2 segment. Therefore, we suggest that the presence or absence of distinct compartments is related both to variations in upper mantle composition and to variations in melting/heterogeneity within the ASP mantle plume.

#### 5.2.4. Interplay Between Upper Mantle and Plume Sources

Given that Pb isotope measurements for basalts older than the most recent stage (stage D  $\leq 0.93$  Ma) are unavailable, several explanations remain possible for the differences between the NW and SE compartments. One simple explanation is that the geographic transition between the Dupal and the mantle (C) components, which approximately corresponds to the length of segment J2, varies in width through the time. In this speculative case, the current 100-km transition may have been smaller in the past, although, in a convecting mantle, a narrower transition seems doubtful unless both mantle sources are immiscible.

Assuming that mantle source provinces remained stable during the last 3 Myr, a second explanation is that the ASP plume material is heterogeneous in volatile/chemical contents. The volatile content of mantle plumes is currently a topic of debate, exemplified by studies in the Azores (i.e., Béguelin et al., 2017; French & Romanowicz, 2015; Métrich et al., 2014). Enrichment in volatiles, specifically water, can lower the mantle solidus temperature and promote higher degrees of partial melting that resemble the effect of higher mantle temperature (Asimow et al., 2004; Bonatti, 1990). In the ASP plume, compositional heterogeneity inferred from the irregular incompatible element concentrations along the SEIR (Figure 5) could be associated with spatially differing volatile contents. Ratios of elements, such as  $\text{H}_2\text{O}/\text{Ce}$ , do not depend on spreading rate or the extent and depth of melting, but they are sensitive to variations in the regional composition of the upper mantle (e.g., Danyushevsky et al., 2000; Dixon et al., 2002; Michael, 1995). The  $\text{H}_2\text{O}/\text{Ce}$  ratio in young SEIR basalts atop the plateau are relatively uniform and have an average of  $200 \pm 16$  (Loewen et al., 2019) and there is no clear correlation between  $\text{H}_2\text{O}/\text{Ce}$  and  $\text{Na}_8$  or  $^3\text{He}/^4\text{He}$  (Figure 5). Notably, one basalt from segment H has  $\text{H}_2\text{O}/\text{Ce}$  ratios that range up to 330 (Figure 5). However, other basalts from the northern part of segment H (outside of our study area) also have  $\text{H}_2\text{O}/\text{Ce}$  ratios higher than 200 (Loewen et al., 2019). Although the data are limited, the elevated  $\text{H}_2\text{O}/\text{Ce}$  ratios along axis segment H basalts are suggested to be related to a recycled water component in the ASP plume that also carries a radiogenic Pb signature yet has relatively primitive He isotope ratios (Loewen et al., 2019). The average  $\text{H}_2\text{O}/\text{Ce}$  ratio obtained for segments I1, I2, and J2 is comparable to average values for N-MORB and E-MORB globally ( $155$  to  $213 \pm 40$ ; Michael, 1995). This seems to indicate an absence of anomalously high  $\text{H}_2\text{O}$  contents



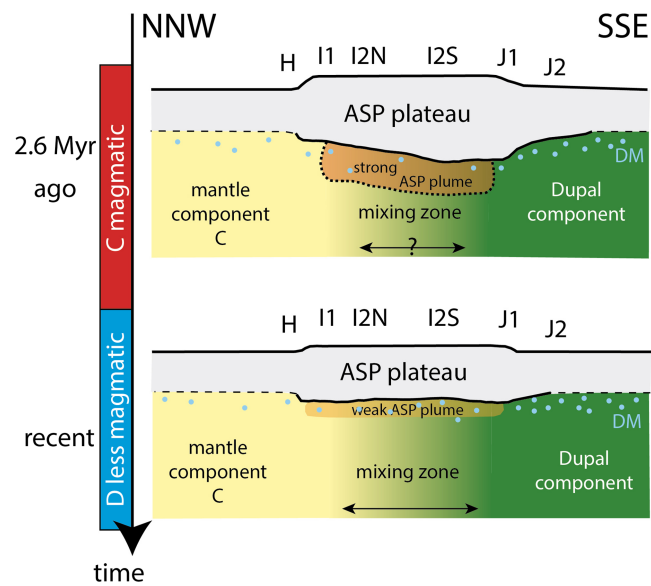


**Figure 7.** Along-axis cartoon of the temporal evolution in mantle sources. The size of the mixing zone at 2.6 Myr is unknown and marked by a question mark. See text for further discussion.

beneath the ASP Plateau, especially in association with the Dupal component in this region. Overall, the observations do not support the hypothesis of a mantle H<sub>2</sub>O anomaly beneath the ASP Plateau (Graham et al., 1999).

Altogether, the evidence suggests that compositional heterogeneity within the ASP mantle plume is partly responsible for the variations in crustal production through time. Relations between  $^3\text{He}/^4\text{He}$ ,  $\epsilon_{\text{Nd}}$ ,  $^{206}\text{Pb}/^{204}\text{Pb}$ , and  $\epsilon_{\text{Hf}}$  reveal that samples from the ASP Plateau (both on- and off-axis) and neighboring segments of the SEIR are mixtures of up to four mantle components (Graham et al., 2014; Nicolaysen et al., 2007). These components include a primitive plume component (having high  $^3\text{He}/^4\text{He}$ ), ambient depleted upper mantle, and recycled crustal/lithospheric materials (Dupal and C components). Mixing between these end-members accounts for the isotopic variability along the ridge segments I1, I2, J1, and J2. In addition, differences in fertility of the individual components may influence magma supply and lead to the observed crustal thickness variations.

## 6. Spatiotemporal Evolution of the Ridge Accretion Pattern During the Last 3 Myr

During the robust magma supply stage (Stage C), heterogeneous ASP plume material was drained toward the ridge axis and mixed with the ambient mantle source, building a robust plateau characterized by high and large abyssal hills (Figures 2 and 7). The ambient mantle source beneath individual ridge segments appears to have had distinct isotopic signatures (Nicolaysen et al., 2007) that correspond to (1) a mantle component C (or common, composition of Hanan & Graham, 1996) to the north (H and I1 segments) accompanied by normal melt production/crustal thickness and (2) a strong Dupal anomaly component to the south (J1 and J2 segment) responsible for thicker crust. Segment I2 appears to show mixing between both of these mantle sources (plus ambient depleted upper mantle, DM; Figures 5 and 7).

Between 2.57 and 1.76 Ma (Figure 4c), there was a reduction in crustal thickness in the SE compartment, suggesting that less plume material arrived at the ridge axis, potentially due to a plume-conduit oscillation. The low-magma supply stage (Stage D) began at this time and the connection between the subridge mantle and the plume weakened. The remaining hot and less-dense plume material was slowly incorporated into the ridge-axis structure. Once the supply of ASP plume material decreased, the thickness of the crust and of the lithosphere decreased. Intriguingly, the thickness of the crust slowly increases to the north. This further suggests that the underlying ASP mantle plume is compositionally heterogeneous, with a more fertile portion situated below the northern part of the ridge axis.

Between 1.76 and 0.8 Ma, the plume flux decreased and melt production reached similar levels within each plateau compartment. Crustal thinning has since occurred along the entire I2 segment (Figure 4c). Bathymetrically, the plateau is also characterized by an abrupt change in faulting style, consistent with a decrease of plume material reaching the axis (Figures 2 and 3). The sigmoidal shape of the transition to a rougher bathymetry having a succession of lower and small abyssal hills and grabens indicates that interaction between heterogeneous shallow mantle and the progressively weaker ASP mantle plume varied through time. Today, the bathymetry along segment I2 is relatively smooth, with a uniform crustal thickness of ~8 km, greater than the normal average of 6 km, suggesting that the ridge is still influenced by the plume (Figure 7).

Similar crustal thicknesses in both compartments also occurred during the previous low magmatic stage (Stage B, Area B; Figure 4a), when the ridge was migrating toward the ASP plume. At around 5 Ma, the minimum thickness reached in both compartments was ~7 km. The slightly thicker crust at 5 Ma relative to the typical spreading ridge average of 6 km may relate to the direction of ridge migration with respect to the plume at that time. Numerical models predict that plume volumes and the amount of magma reaching the ridge axis depend on the ridge migration direction (Ito et al., 1999; Ribe & Delattre, 1998). There are a number of examples of ridges moving away from a plume while still maintaining a flow connection, such as along the Central Indian Ridge (Morgan, 1978) and the Easter Microplate (Kingsley & Schilling, 1998; Pan & Batiza, 1998). Geochemical and geophysical studies led to the so-called “hot spot source-migrating ridge sink model” (Schilling, 1985) where the ridge acts as a sink draining plume material along a narrow sublithospheric channel. Both the numerical results and the observations suggest that for a given plume-ridge distance, the predicted amount of melting is higher when a ridge is migrating away from a plume, and this generates thicker crust than when a ridge is approaching a plume.

We can speculate about the further evolution of the ASP Plateau, assuming the current location of the ASP mantle plume between the islands of Amsterdam and St. Paul, where the helium anomaly is highest (~14.1; Nicolaysen et al., 2007). Today, plume-ridge distance is estimated at 65 km and increasing as the ridge continues to migrate to the northeast (Maia et al., 2011). Using scaling results from analytical models (Ribe & Delattre, 1998), the maximum plume/ridge interaction distance for the ASP plume can be estimated at 255 km. At current spreading and ridge migration rates relative to the plume, this distance will be reached in ~2.4 Myr. Compared to the 3-Myr pulse duration, a new stage of magmatic construction begins at the inception of a plume oscillation. Moreover, the I2 ridge segment has jumped twice in the last 10 Myr. The second jump occurred at 3.3 Ma during a low magmatic supply stage like the one today. A future ridge jump could again reduce the distance between the plume and the ridge axis and facilitate a resumption of robust volcanic construction.

## 7. Summary and Conclusions

We present observations and analysis of bathymetry and gravity data collected during the BOOMERANG and PLURIEL expeditions to the region of the Amsterdam-St. Paul Plateau. Coupled with available and new geochemical data, we characterize a region of anomalous crustal thickness related to the nearby Amsterdam-St. Paul hot spot and shallow upper mantle sources, which have dominated the 3-D morphological architecture of the plateau.

Bathymetry and gravity data reveal significant variations in morphology and crustal thickness across the ASP Plateau and along the nearby SEIR axis since 10 Ma. We observe two periods of increased melt supply at the SEIR axis associated with thick crust and smooth, axial high-type morphologies. The two periods are separated by a low magmatic phase, where the crust thickness is closer to the 6-km global average value and the morphology is of a rift valley type. This variation in melt production reveals temporal variations in ASP plume flux that may have been associated with oscillations in the plume conduit. This conclusion strengthens the model of Maia et al. (2011) in which the variations in plume fluxes can also promote ridge axis jumps.

Bathymetry and gravity data also show that during both stages of strong magmatic activity, crustal thickness was smaller in stage A than in stage C. This difference in crustal production is explained by migration of the SEIR over a fixed ASP hot spot. For the same plume-ridge distance, crust is thicker when the ridge recedes from the plume than when the ridge approaches the plume.

Melt production has been variable along the ridge axis, leading to the separation of segment I2 into two distinct compartments. Over the last 10 Myr, the SE compartment displays thicker crust and shallower water depths than the NW compartment. The morphology and crustal thickness characteristics of both compartments covary with 8/4Pb values. The 8/4Pb in basalts from the southern part of the I2 segment is high and consistent with a strong Dupal anomaly. In contrast, basalts from the northern segment have significantly lower 8/4Pb values. This pattern suggests that isotopic and chemical heterogeneity in the plume or the upper mantle, or both, accounts for the differences in melt production between the NW and the SE compartments. Moreover, K/Ti and  $^3\text{He}/^4\text{He}$  peaks are symmetric along the SEIR atop the ASP Plateau, while 8/4Pb decreases smoothly northward from 110 to 60. We propose that the variation in 8/4Pb is not only related to the ASP plume's influence but that it also reflects isotopic variability in the upper mantle beneath the plateau.

Since 3 Ma, gravity-derived crustal thickness decreased earlier in the SE (~1.42 Ma) than in the NW (~0.93 Ma). Moreover, comparing bathymetry and gravity between segments H to J2 reveals that variations in melt production relative to distinct mantle sources (represented by different 8/4Pb values) are sensitive to the upwelling rate. Indeed, during the present low magmatic period, there is no discernible difference between the NW and SE compartments. Changes in the distinction of compartments through time and asynchronous thinning of the crust could indicate a plume with a heterogeneous distribution of volatiles and a compositional zonation.  $\text{H}_2\text{O}/\text{Ce}$  ratios across the SEIR are comparable to normal upper mantle and do not support crustal variability arising from different contributions of a “wet” plume source. However, differential melting of a hybridized mantle containing several geochemical components (a primitive mantle plume component, ambient depleted upper mantle, and recycled crustal/lithospheric materials tracked by the Dupal and C components) explains the variability in along-axis melt production during the last 3 Myr.

The crustal structure and seafloor morphology are controlled by chemical variability in the underlying mantle during interaction of the intermediate spreading ridge and the relatively weak ASP mantle plume. On the ASP Plateau, the along-axis temporal variations in crustal thickness and seafloor morphology are explained by temporal and/or geographic variability in the different mantle source materials being tapped by the I2 segment. However, important details of these variations remain somewhat unclear, and require additional chemical and isotopic studies of older basalts (>1 Ma) in the region.

## Acknowledgments

This work was supported by an international postdoctoral grant of the “Laboratoire d’Excellence” LabexMER. The PLURIEL cruise was funded through a grant to the Flotte Océanographique Française and CNRS-INSU. The BOOMERANG 06 expedition was funded by the the National Science Foundation through grant OCE-9505667 of the RIDGE Initiative. E.M. was supported by grant EAR-1520856. D.G. was supported by OCE1558798 and 1763255 from NSF. The authors would like to thank A. Davaille for the fruitful discussions. We thank the Editor Thorsten Becker and the three anonymous reviewers for the comments that improved the quality of this work. Methods, including statements of data availability, are available in the main manuscript, in figures and tables provided in the supporting information, and at this url: <https://mycore.core-cloud.net/index.php/s/6N9zwSyYPG1DIPS>.

## References

- Adam, C., Vidal, V., & Escartin, J. (2007). 80-Myr history of buoyancy and volcanic fluxes along the trails of the Walvis and St. Helena hotspots (South Atlantic). *Earth and Planetary Science Letters*, 261, 432–442.
- Allen, R. M., Nolet, G., Jason Morgan, W., Vogt, K., Bergsson, B. H., Erlendsson, P., et al. (2002). Imaging the mantle beneath Iceland using integrated seismological techniques. *Journal of Geophysical Research*, 107(B12), 2325. <https://doi.org/10.1029/2001JB000595>
- Asimow, P. D., Dixon, J. E., & Langmuir, C. H. (2004). A hydrous melting and fractionation model for mid-ocean ridge basalts: Application to the Mid-Atlantic Ridge near the Azores. *Geochemistry, Geophysics, Geosystems*, 5, Q01E16. <https://doi.org/10.1029/2003GC000568>
- Béguélin, P., Bizimis, M., Beier, C., & Turner, S. (2017). Rift-plume interaction reveals multiple generations of recycled oceanic crust in Azores lavas. *Geochemica et Cosmochimica Acta*, 218, 132–152.
- Behn, M. D., & Ito, G. (2008). Magmatic and tectonic extension at mid-ocean ridges: 1. Controls on fault characteristics. *Geochemistry, Geophysics, Geosystems*, 9, Q08O10. <https://doi.org/10.1029/2008GC001965>
- Bonatti, E. (1990). Not so hot “hot spots” in the oceanic mantle. *Science*, 250, 107–110.
- Braun, M. G., & Sohn, R. A. (2003). Melt migration in plume-ridge systems. *Earth and Planetary Science Letters*, 213(3–4), 417–430.
- Brozena, J. M., & White, R. S. (1990). Ridge jumps and propagations in the South Atlantic Ocean. *Nature*, 348, 149–152.
- Buck, W. R., Lavier, L. L., & Poliakov, A. N. B. (2005). Modes of faulting at mid-ocean ridges. *Nature*, 434(7034), 719–723. <https://doi.org/10.1038/nature03358>
- Canales, J. P., Danobeitia, J. J., Detrick, R. S., Hooft, E. E. E., Barolomé, R., & Naar, D. (1997). Variations in axial morphology along the Galapagos Spreading Center and the influence of the Galapagos hotspot. *Journal of Geophysical Research*, 102(B12), 27,341–27,354. <https://doi.org/10.1029/97JB01633>
- Cannat, M., Briais, A., Deplus, C., Escartin, J., Geogren, J., Lin, J., et al. (1999). Mid-Atlantic Ridge-Azores hotspot interactions: along-axis migration of a hotspot-derived event of enhanced magmatism 10 to 4 Ma ago. *Earth and Planetary Science Letters*, 173, 257–269.
- Carbotte, S. M., Samll, C., & Donnelly, K. (2004). The influence of ridge migration on the magmatic segmentation of mid-ocean ridges. *Nature*, 429(6993), 743–746. <https://doi.org/10.1038/nature02652>
- Chen, Y. J. (1996). Constraints on the melt production rate beneath the mid-ocean ridges based on passive flow models. *Pure and Applied Geophysics*, 146, 589–620. <https://doi.org/10.1007/B00874735>
- Chen, Y. J., & Lin, J. (2004). High sensitivity of ocean ridge thermal structure to changes in magma supply: The Galapagos Spreading Center. *Earth and Planetary Science Letters*, 221, 263–273.
- Conder, J. A., Scheirer, D. S., & Forsyth, D. W. (2000). Seafloor spreading on the Amsterdam-St. Paul hotspot plateau. *Journal of Geophysical Research*, 105(B4), 8263–8277. <https://doi.org/10.1029/1999JB900406>
- Courrèges, E. (2010). Plateaux de St-Paul Amsterdam et Nord Kerguelen: interaction entre la dorsale SE indienne et des points chauds. PhD thesis, Univ. Bretagne Occidentale. 235pp.

- Cushman, B., Sinton, J., Ito, G., & Eaby Dixon, J. (2004). Glass compositions, plume-ridge interaction, and hydrous melting along the Galapagos Spreading Center, 90.5°W to 98°W. *Geochemistry, Geophysics, Geosystems*, 5, Q08E17. <https://doi.org/10.1029/2004GC000709>
- Dalton, C. A., Langmuir, C. H., & Gale, A. (2014). Geophysical and geochemical evidence for deep temperature variations beneath mid-ocean ridges. *Science*, 344(6179), 80–83. <https://doi.org/10.1126/science.1249466>
- Danyushevsky, L. V., Eggins, S. M., Falloon, T. J., & Christie, D. M. (2000). H<sub>2</sub>O abundance in depleted to moderately enriched mid-ocean ridge magmas; Part I: Incompatible behaviour, implications for mantle storage, and origin of regional variations. *Journal of Petrology*, 41, 1329–1364.
- Deschamps, A., Shinjo, R., Matsumoto, T., Lee, C.-S., Lallemand, S. E., Wu, S., & Scientific party of KR03-04 and KR04-14 cruises (2008). Propagators and ridge jumps in a back-arc basin, the West Philippine Basin. *Terra Nova*, 20, 327–332.
- Dixon, J. E., Leist, L., Langmuir, C., & Schilling, J.-G. (2002). Recycled dehydrated lithosphere observed in plume-influenced mid-ocean ridge basalt. *Nature*, 420(6914), 385–389. <https://doi.org/10.1038/nature01215>
- Douglas-Priebe, L.M. (1998). Geochemical and petrogenetic effects of the interaction of the Southeast Indian Ridge and the Amsterdam-Saint Paul hotspot. M.S. thesis, Oregon State University, Corvallis. 132p.
- Dupré, B., & Allègre, C. J. (1983). Pb-Sr isotope variation in Indian Ocean basalts and mixing phenomena. *Nature*, 303, 142–146.
- French, S. W., & Romanowicz, B. (2015). Broad plumes rooted at the base of the Earth's mantle beneath major hotspots. *Nature*, 525, 95–99.
- Gente, P., Dymet, J., Maia, M., & Goslin, J. (2003). Interaction between the Mid-Atlantic Ridge and the Azores hot spot during the last 85 Myr: Emplacement and rifting of the hot spot-derived plateaus. *Geochemistry, Geophysics, Geosystems*, 4(10), 8514. <https://doi.org/10.1029/2003GC000527>
- Graham, D. W., Hanan, B. B., Hémond, C., Blichert-Toft, J., & Albarède, F. (2014). Helium isotopic textures in Earth's upper mantle. *Geochemistry, Geophysics, Geosystems*, 15, 2048–2074. <https://doi.org/10.1002/2014GC005264>
- Graham, D. W., Johnson, K. T. M., Priebe, L. D., & Lupton, J. E. (1999). Hotspot-ridge interaction along the Southeast Indian Ridge near Amsterdam and St. Paul Islands: Helium isotope evidence. *Earth and Planetary Science Letters*, 167, 297–310.
- Hanan, B. B., & Graham, D. W. (1996). Lead and helium isotope evidence from oceanic basalts for a common deep source of mantle plumes. *Science*, 272(5264), 991–995. <https://doi.org/10.1126/science.272.5264.991>
- Hanan, B. B., & Schilling, J.-G. (1997). The dynamic evolution of the Iceland mantle plume: the lead isotope perspective. *Earth and Planetary Science Letters*, 151(1-2), 43–60.
- Hardarson, B. S., Fitton, J. G., Ellam, R. M., & Pringle, M. S. (1997). Rift relocation – A geochemical and geochronological investigation of a paolo-rift in northwest Iceland. *Earth and Planetary Science Letters*, 153, 181–196.
- Hart, S. R. (1984). A large-scale isotope anomaly in the Southern Hemisphere mantle. *Nature* 309, 753–757.
- Hebert, L. B., & Montési, L. G. J. (2011). Melt extraction pathways at segmented oceanic ridges: Application to the East Pacific Rise at the Siqueiros transform. *Geophysical Research Letters*, 38, L11306. <https://doi.org/10.1029/2011GL047206>
- Hey, R., Johnson, J. L., & Lowrie, A. (1977). Recent plate motions in the Galapagos area. *Geological Society of America Bulletin*, 88, 1385–1403.
- Hey, R. N., & Vogt, P. J. (1977). Spreading center jumps and subaxial asthenospheric flow near the Galapagos hot spot. *Tectonophysics*, 37, 41–52.
- Hirschmann, M. M., & Stolper, E. M. (1996). A possible role for garnet pyroxenite in the origin of the “garnet signature” in MORB. *Contributions to Mineralogy and Petrology*, 124(2), 185–208.
- Ito, G. (2001). Reykjanes “V”-shaped roddes originating from a pulsing and dehydrating mantle plume. *Nature*, 411(6838), 681–684. <https://doi.org/10.1038/35079561>
- Ito, G., & Behn, M. D. (2008). Magmatic and tectonic extension at mid-ocean ridges: 2. Origin of axial morphology. *Geochemistry, Geophysics, Geosystems*, 9, Q08O10. <https://doi.org/10.1029/2008GC001965>
- Ito, G., Lin, J., & Gable, C. W. (1997). Interaction of mantle plumes and migrating mid-ocean ridges: Implications for the Galapagos plume-ridge system. *Journal of Geophysical Research*, 102(B7), 15,403–15,417. <https://doi.org/10.1029/97JB01049>
- Ito, G., Lin, J., & Graham, D. (2003). Observational and theoretical studies of the dynamics of mantle plume-mid-ocean ridge interaction. *Reviews of Geophysics*, 41(4), 1017. <https://doi.org/10.1029/2002RG000117>
- Ito, G., Shen, Y., Hirth, G., & Wolfe, C. (1999). Mantle flow, melting, and dehydration of the Iceland mantle plume. *Earth and Planetary Science Letters*, 165, 81–96.
- Janin, M., Hémond, C., Guillou, H., Maia, M., Johnson, K. T. M., Bollinger, C., Liorzou, C., et al. (2011). Hot spot activity and tectonic settings near Amsterdam-St. Paul plateau (Indian Ocean). *Journal of Geophysical Research*, 116, B05206. <https://doi.org/10.1029/2010JB007800>
- Johnson, G. L., Southall, J. R., Young, P. W., & Vogt, P. R. (1972). Origin and structure of the Iceland Plateau and Kolbeinsey Ridge. *Journal of Geophysical Research*, 77(29), 5688–5696. <https://doi.org/10.1029/JB077i029p05688>
- Johnson, K. T. M., Graham, D. W., Rubin, H., Nicolaysen, K., Scheirer, D. S., Forsyth, E. T., & Douglas-Priebe, L. M. (2000). Boomerang Seamount: The active expression of the Amsterdam-St Paul hotspot, Southeast Indian Ridge. *Earth and Planetary Science Letters*, 183, 245–259.
- Karsten, J. L., & Delaney, J. R. (1989). Hot spot-ridge crest convergence in the northeast Pacific. *Journal of Geophysical Research*, 94(B1), 700–712. <https://doi.org/10.1029/JB094iB01p00700>
- Kingsley, R. H., & Schilling, J.-G. (1998). Plume-ridge interaction in the Easter-Salas y Gomez seamount chain-Easter Microplate system: Pb isotope evidence. *Journal of Geophysical Research*, 103(B10), 24,159–24,177. <https://doi.org/10.1029/98JB01496>
- Klein, E. M., & Langmuir, C. H. (1987). Global correlations of ocean ridge basalt chemistry with axial depth and crustal thickness. *Journal of Geophysical Research*, 92(B8), 8089–8115. <https://doi.org/10.1029/JB092iB08p08089>
- Kuo, B.-Y., & Forsyth, D. W. (1988). Gravity anomalies of the ridge-transform system in the South Atlantic between 31 and 34.5°S: Upwelling centers and variations in crustal thickness. *Marine Geophysical Researches*, 10, 205–232.
- Kurz, M. D., Jenkins, W. J., & Hart, S. R. (1982). Helium isotopic systematics of oceanic islands: implications for mantle heterogeneity. *Nature*, 297, 43–47.
- Langmuir, C. H., Klein, E. M., & Plank, T. (1992). Petrological systematics of mid-ocean ridge basalts: Constraints on melt generation beneath ocean ridges. In J. Phipps Morgan, D. K. Blackman, & J. M. Sinton (Eds.), *Mantle Flow and Melt generation at Mid-ocean Ridges*, *Geophys. Monogr. Ser.* (Vol. 71, pp. 183–280). Washington, DC: American Geophysical Union.
- Loewen, M. W., Graham, D. W., Bindeman, I. N., Lupton, J. E., & Garcia, M. O. (2019). Hydrogen isotopes in high <sup>3</sup>He/<sup>4</sup>He submarine basalts: Primordial vs. recycled water and the veil of mantle enrichment. *Earth and Planetary Science Letters*, 508, 62–73.



- Lupton, J. E. (1983). Terrestrial inert gases: Isotope tracer studies and clues to primordial components in the mantle. *Annual Review of Earth and Planetary Sciences*, 11, 371–414.
- Magde, L. S., & Sparks, D. W. (1997). Three-dimensional mantle upwelling, melt generation, and melt migration beneath segment slow spreading ridges. *Journal of Geophysical Research*, 102(B9), 20,571–20,583. <https://doi.org/10.1029/97JB01278>
- Maia, M., Ackermann, D., Dehghani, G. A., Gente, P., Hékinian, R., Naar, D., et al. (2000). The Pacific-Antarctic Ridge–Foundation hotspot interaction: a case study of a ridge approaching a hotspot. *Marine Geology*, 167(1–2), 61–84. [https://doi.org/10.1016/S0025-3227\(00\)00023-2](https://doi.org/10.1016/S0025-3227(00)00023-2)
- Maia, M., Goslin, J., & Gente, P. (2007). Evolution of the accretion processes along the Mid-Atlantic Ridge north of the Azores since 5.5 Ma: An insight into the interactions between the ridge and the plume. *Geochemistry, Geophysics, Geosystems*, 8, Q03013. <https://doi.org/10.1029/2006GC001318>
- Maia, M., Hémond, C., & Gente, P. (2001). Contrasted interactions between plume, upper mantle, and lithosphere: Foundation chain case. *Geochemistry, Geophysics, Geosystems*, 2(7), 1028. <https://doi.org/10.1029/2000GC000117>
- Maia, M., Pessanha, I., Courrèges, E., Patriat, M., Gente, P., Hémond, C., et al. (2011). Building of the Amsterdam-Saint Paul plateau: A 10 Myr history of a ridge-hot spot interaction and variations in the strength of the hot spot source. *Journal of Geophysical Research*, 116, B09104. <https://doi.org/10.1029/2010JB007768>
- Maiden, M. D., & Hoefer, M. A. (2016). Modulations of viscous fluid conduit periodic waves. *Proceedings of the Royal Society A: Mathematical, Physical and Engineering Sciences*, 472, 20160533. <https://doi.org/10.1098/rspa.2016.0533>
- McKenzie, D. (1984). The generation and compaction of partially molten rock. *Journal of Petrology*, 25, 713–765.
- Métrich, N., Zanon, V., Créon, L., Hildenbrand, A., Moreira, M., & Marques, F. O. (2014). Is the ‘Azores Hotspot’ a Wetspot? Insights from the geochemistry of fluid and melt inclusions in olivine of pico basalts. *Journal of Petrology*, 55, 377–393.
- Michael, P. (1995). Regionally distinctive sources of depleted MORB: Evidence from trace elements and H<sub>2</sub>O. *Earth and Planetary Science Letters*, 131, 301–320.
- Mittelstaedt, E., Ito, G., & van Hunen, J. (2011). Repeat ridge jumps associated with plume-ridge interaction, melt transport, and ridge migration. *Journal of Geophysical Research*, 116, B01102. <https://doi.org/10.1029/2010JB007504>
- Mittelstaedt, E., Soule, S., Harpp, K., Fornari, D., McKee, C., Tivey, M., et al. (2012). Multiple expressions of plume-ridge interaction in the Galapagos: Volcanic lineaments and ridge jumps. *Geochemistry, Geophysics, Geosystems*, 13, Q05018. <https://doi.org/10.1029/2012GC004093>
- Mjelde, R., Breivik, A. J., Raum, T., Mittelstaedt, E., Ito, G., & Faleide, J. I. (2008). Magmatic and tectonic evolution of the North Atlantic. *Journal of the Geological Society*, 165, 31–42. <https://doi.org/10.1144/0016-76492007-018>
- Montési, L. G. J., Behn, M. D., Hebert, L. B., Lin, J., & Barry, J. L. (2011). Controls on melt migration and extraction at the ultraslow Southwest Indian Ridge 10°–16°E. *Journal of Geophysical Research*, 116, B10102. <https://doi.org/10.1029/2011JB008259>
- Morgan, W. J. (1978). Rodriguez, Darwin, Amsterdam, ... A second type of hotspot island. *Journal of Geophysical Research*, 83(B11), 5355–5360. <https://doi.org/10.1029/JB083iB11p05355>
- Neuharth, D., & Mittelstaedt, E. (2017). Temporal variations in hotspot volcanic production caused by interactions between upwelling mantle plumes and phase transitions. Abstract D111A-0262 presented at 2017 Fall Meeting, AGU, New Orleans, L.A., 11–15 dec.
- Nicolaysen, K. P., Frey, F. A., Mahoney, J. J., Johnson, T. M., & Graham, D. W. (2007). Influence of the Amsterdam/St. Paul hot spot along the Southeast Indian Ridge between 77° and 88°E: Correlations of Sr, Nd, Pb, and He isotopic variations with ridge segmentation. *Geochemistry, Geophysics, Geosystems*, 8, Q09007. <https://doi.org/10.1029/2006GC001540>
- Olson, P., & Singer, H. (1985). Creeping plumes. *Journal of Fluid Mechanics*, 158, 511–531.
- Pan, Y., & Batiza, R. (1998). Major element chemistry of volcanic glasses from the Easter Seamount Chain: Constraints on melting conditions in the plume channel. *Journal of Geophysical Research*, 103(B3), 5287–5304. <https://doi.org/10.1029/97JB03617>
- Parsons, B., & Sclater, J. G. (1977). An analysis of the variation of ocean floor bathymetry and heat flow with age. *Journal of Geophysical Research*, 82(5), 803–827. <https://doi.org/10.1029/JB082i005p0803>
- Phipps Morgan, J., & Chen, Y. J. (1993). The genesis of oceanic crust: Magma injection, hydrothermal circulation, and crustal flow. *Journal of Geophysical Research*, 98(B4), 6283–6297. <https://doi.org/10.1029/92JB02650>
- Ribe, N., & Delattre, W. L. (1998). The dynamics of plume-ridge interaction, 3: The effects of ridge migration. *Geophysical Journal International*, 133, 511–518.
- Scheirer, D. S., Forsyth, D. W., Conder, J. A., Eberle, M. A., Hung, S.-H., Johnson, T. L., & Graham, D. W. (2000). Anomalous seafloor spreading of the Southeast Indian Ridge near the Amsterdam-St. Paul Plateau. *Journal of Geophysical Research*, 105(B4), 8243–8262. <https://doi.org/10.1029/1999JB900407>
- Schilling, J.-G. (1985). Upper mantle heterogeneities and dynamics. *Nature*, 314, 62–67.
- Schilling, J.-G. (1991). Fluxes and excess temperatures of mantle plumes inferred from their interaction with migrating mid-ocean ridges. *Nature*, 352, 397–403.
- Schilling, J.-G., Kingsley, R. H., & Devine, J. D. (1982). Galapagos Hot Spot-Spreading Centre System. 1. Spatial petrological and geochemical variations (83°W–101°W). *Journal of Geophysical Research*, 87(B7), 5593–5610. <https://doi.org/10.1029/JB087iB07p05593>
- Schilling, J.-G., & Noe-Nygaard, A. (1974). Faeroe-Iceland plume: Rare-Earth evidence. *Earth and Planetary Science Letters*, 24, 1–14.
- Schilling, J.-G., Zajac, M., Evans, R., Johnson, T., White, W., Devine, J. D., & Kingsley, R. (1983). Petrologic and geochemical variations along the Mid-Atlantic Ridge from 29°N to 73°N. *American Journal of Science*, 283, 510–586.
- Schubert, G., Olson, P., Anderson, C., & Goldman, P. (1989). Solitary waves in mantle plumes. *Journal of Geophysical Research*, 94(B7), 9523–9532. <https://doi.org/10.1029/JB094iB07p09523>
- Scott, D. R., Stevenson, D. J., & Whitehead, J. A. (1986). Observations of solitary waves in a viscously deformable pipe. *Nature*, 319, 759–761.
- Sibrant, A. L. R., Mittelstaedt, E., Davaille, A., Pauchard, L., Aubertin, A., Auffray, L., & Pidoux, R. (2018). Accretion mode of oceanic ridges governed by axial mechanical strength. *Nature Geoscience*, 11(4), 274–279. <https://doi.org/10.1038/s41561-018-0084-x>
- Sparks, D. W., & Parmentier, E. M. (1991). Melt extraction from the mantle beneath spreading centers. *Earth and Planetary Science Letters*, 105(4), 368–377. [https://doi.org/10.1016/0012-821X\(91\)90178-K](https://doi.org/10.1016/0012-821X(91)90178-K)
- Sparks, D. W., Parmentier, E. M., & Phipps Morgan, J. (1994). Three dimensional mantle convection beneath a segmented spreading center: Implications for along-axis variations in crustal thickness and gravity. *Journal of Geophysical Research*, 98, 21,977–21,995. <https://doi.org/10.1029/93jb02397>
- Stein, C. A., & Stein, S. (1992). A model for the global variation in oceanic depth and heat flow with lithospheric age. *Nature*, 359, 123–129.
- Steinberger, B. (2000). Plumes in a convecting mantle: Models and observations for individual hotspots. *Journal of Geophysical Research*, 105(B5), 11,127–11,152. <https://doi.org/10.1029/1999JB900398>
- Turcotte, D. L., & Schubert, G. (2002). *Geodynamics* (2nd ed.p. 456). New York: Cambridge University Press.



- Vogt, P. R. (1976). Plumes, subaxial pipe flow, and topography along the mid-ocean ridge. *Earth and Planetary Science Letters*, 29, 309–325.
- Weiss, Y., Class, C., Goldstein, S. L., & Hanyu, T. (2016). Key new pieces of the HIMU puzzle from olivines and diamond inclusions. *Nature*, 537(7622), 666–670. <https://doi.org/10.1038/nature19113>
- White, W. M., & Schilling, J.-G. (1978). The nature and origin of geochemical variation in Mid-Atlantic Ridge basalts from the Central North Atlantic. *Geochimica et Cosmochimica Acta*, 42(10), 1501–1516.
- Whitehead, J. A. (1982). Instabilities of fluid conduits in a flowing earth – are plates lubricated by the asthenosphere? *Geophysical Journal of the Royal Astronomical Society*, 70, 415–433.
- Zhao, D. (2007). Seismic images under 60 hotspots: Search for mantle plumes. *Gondwana Research*, 12, 335–355.